

Bloch oscillations and the lack of the decay of the false vacuum in a one-dimensional quantum spin chain

O. Pomponio^{1,2}, M.A. Werner^{3,4}, G. Zaránd^{3,4} and G. Takács³

¹Dipartimento di Fisica e Astronomia dell'Università di Bologna

Via Irnerio 46, 40126 Bologna, Italy

²Istituto Nazionale di Fisica Nucleare, Sezione di Bologna

Via Irnerio 46, 40126 Bologna, Italy

³BME-MTA Exotic Quantum Phases 'Lendület' Research Group

Budapest University of Technology and Economics, 1111 Budapest, Budafoki út 8, Hungary

⁴MTA-BME Quantum Correlations Group, Department of Theoretical Physics,

Budapest University of Technology and Economics, 1111 Budapest, Budafoki út 8, Hungary

30th April 2021

Abstract

We consider the decay of the false vacuum, realised within a quantum quench into an anti-confining regime of the Ising spin chain with a magnetic field opposite to the initial magnetisation. Although the effective linear potential between the domain walls is repulsive, the time evolution of correlations still shows a suppression of the light cone and a reduction of vacuum decay. The suppressed decay is a lattice effect, and can be assigned to emergent Bloch oscillations.

1 Introduction

Quantum quenches, i.e., sudden changes in a system's Hamiltonian [1,2] provide a paradigmatic protocol to study non-equilibrium quantum dynamics and relaxation in by now routinely engineered closed quantum systems [3–10]. In global, translationally invariant quantum quenches, the initial state has a finite uniform energy density with respect to the post-quench Hamiltonian, and the system is therefore in a highly excited state. This highly excited configuration acts as a *source* of quasi-particle excitations, which may collide and thermalize with time. Indeed, within a semi-classical picture [1], these quasi-particle excitations drive equilibration by spreading correlation and entanglement across the system.

In a large class of systems, including various spin chains with short-range interactions, or interacting bosonic or fermionic systems, quasi-particles have an upper bound on their velocity [11], leading typically to a distinctive light-cone pattern in time dependent correlation functions [1,2,12–17]. This behavior is, however, not completely generic: confining forces, as a remarkable exception, can suppress the light-cone spreading of correlations [18]. The prediction of *dynamical confinement* has indeed been confirmed recently in numerous systems and settings exhibiting confinement [19–28].

Dynamical confinement [18] has originally been observed in the ferromagnetic phase ($g < 1$)

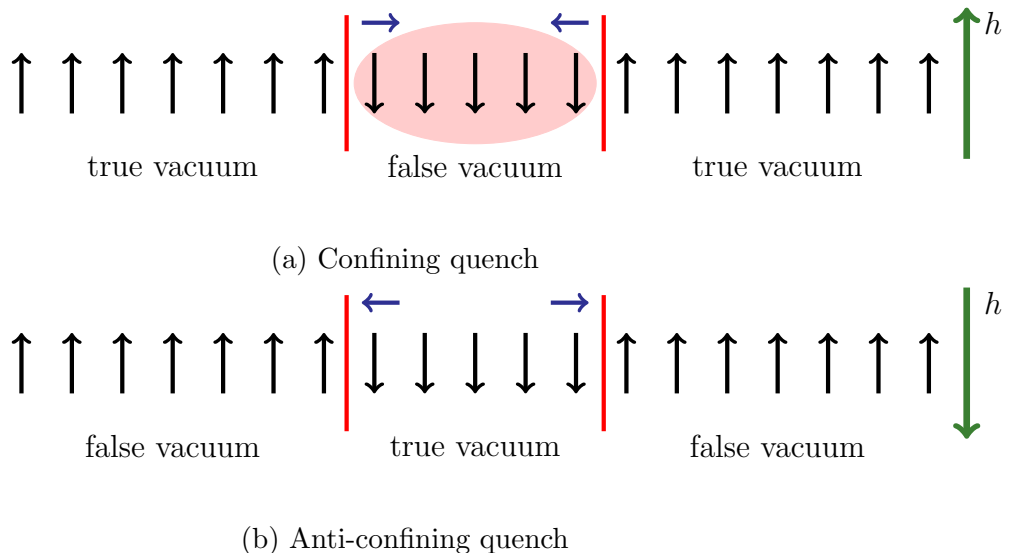


Figure 1.1: (a) For the longitudinal field h parallel to the initial magnetisation, bubbles nucleated during the quench contain the false vacuum. The corresponding attractive forces (blue arrows), confine domain walls (indicated by red lines) into ‘mesons’. (b) For h opposite to the initial magnetisation, the nucleating bubbles contain the true vacuum. The induced repulsive force accelerates the domain walls outwards.

of the quantum Ising spin chain, governed by the Hamiltonian

$$H_{\text{QISC}} = -J \sum_{i=0}^{L-1} (\sigma_i^z \sigma_{i+1}^z + g \sigma_i^x + h \sigma_i^z). \quad \sigma_{i+L}^\alpha \equiv \sigma_i^\alpha,$$

Dynamical confinement occurs while initializing the system in its $g_0 < 1$ positive (spontaneous) magnetisation ground state with $m = \langle \sigma_i^z \rangle > 0$ and $h_0 = 0$, and then quenching to a Hamiltonian with some $g < 1$ and $h > 0$. In this case, the quench gives rise to oppositely moving domain walls (kink-antikink pairs), with a ‘bubble’ of negative magnetisation $-m$ stretched between them (see Fig. 1.1). With the magnetic field being turned on in the opposite direction, these bubbles are filled with the ‘false vacuum’, and cost therefore a potential energy that is proportional to the distance between domain walls. The corresponding confining force [29] inhibits the propagation of particles to large distances, and prevents thermalisation of the system within all time scales accessible to numerical simulations.

It is intriguing to ask what happens if we switch on a field $h < 0$. In this case, the initial state becomes the ‘false vacuum’, and the interior of the bubble is filled with the ‘true vacuum’. Therefore, the external field *promotes* the expansion of bubbles, and generates a repulsive force between the domain walls, as illustrated in Fig. 1.1. In quantum field theory, this corresponds to a scenario proposed by Coleman, known as the decay of the false vacuum [30, 31]: the expansion of the bubbles should rapidly accelerate to a maximal velocity, and the true vacuum should fill the entire space. Coleman’s scenario would thus imply in our case that the bubbles should extend to the whole spin chain, which should rapidly relax to an equilibrium or steady state around the true vacuum.

Here we show that Coleman’s scenario is violated in the Ising spin chain. The dynamics of spin-spin correlation function clearly indicate that bubbles do not expand infinitely. Rather, the repulsive force leads to an oscillatory motion of the domain walls, known as Bloch oscillations. These findings are corroborated by recent numerical studies of the order parameter statistics in the quantum Ising spin chain [32].

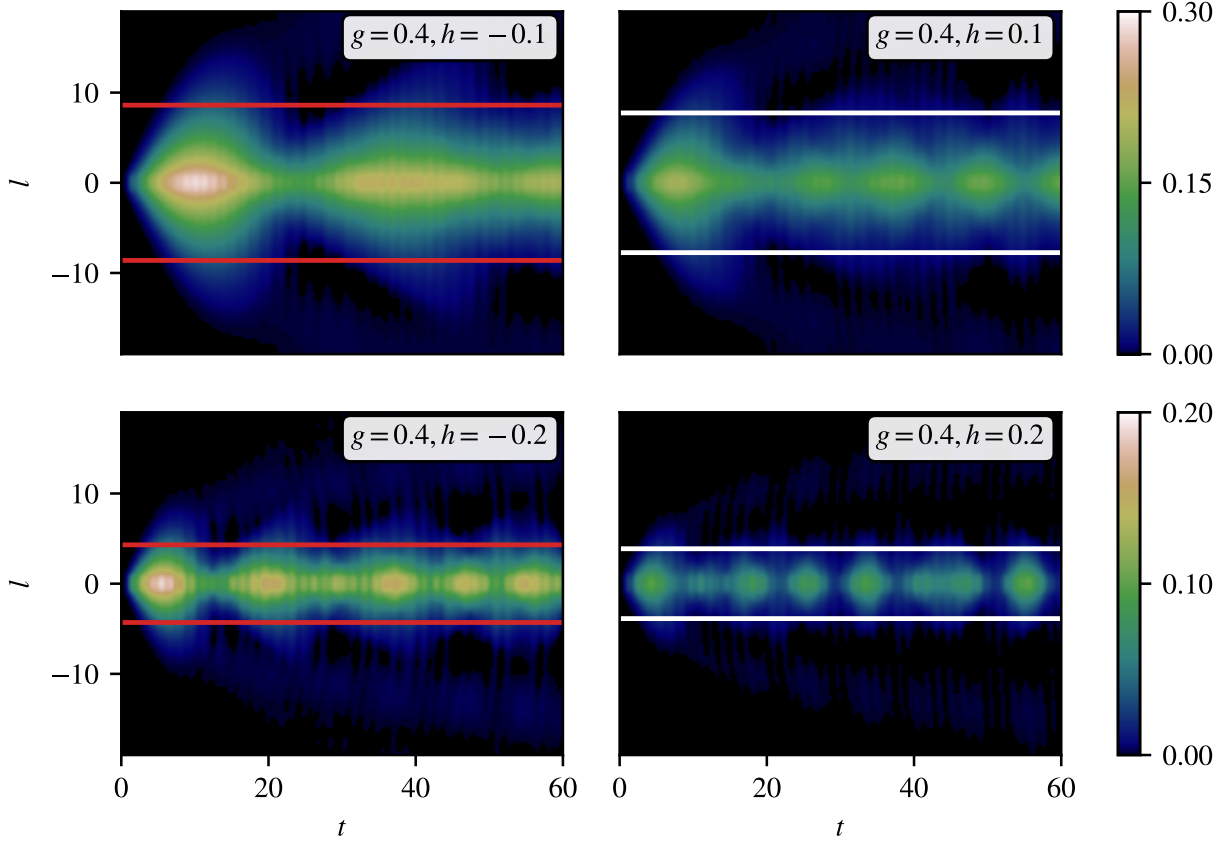


Figure 2.1: Time evolution of the connected spin-spin correlation function $C_z(l, t) \equiv \langle \sigma_0^z(t) \sigma_l^z(t) \rangle_c$ for $g = 0.4$ and for values $h < 0$ (left panel) and $h > 0$ (right panel). The red vs. white lines show the average bubble sizes estimated as in eqn. (2.9) and (2.10) respectively.

2 Dynamics in the anti-confining regime

2.1 Quench setup and subsequent time evolution

As discussed in the introduction, we consider quantum quenches in the ferromagnetic phase. For simplicity, we start the quench from a fully aligned, positively polarised state, i.e. from the ground state with $g_0 = 0$ and $h_0 = 0$. We then quench to a finite transverse field, $g < 1$, and an “anti-confining” longitudinal field $h < 0$. Turning on a finite $g_0 \rightarrow g > 0$ creates a gas of domain wall excitations, which then move in the presence of the field $h < 0$.

The time evolution is numerically simulated using the infinite volume time evolving block decimation (iTEBD) method [33], which we also use to compute the time evolution of the connected two-point equal time spin correlation function

$$C_z(l, t) \equiv \langle \sigma_0^z(t) \sigma_l^z(t) \rangle_c = \langle \sigma_0^z(t) \sigma_l^z(t) \rangle - \langle \sigma_0^z(t) \rangle \langle \sigma_l^z(t) \rangle. \quad (2.1)$$

As shown in Fig. 2.1, at a first sight, the time evolution of $C_z(l, t)$ is remarkably similar for an anti-confining field, $h < 0$, to the one obtained in the dynamical confinement region, $h > 0$, studied in [18]: in both cases, the light-cone propagation of correlations is suppressed, and oscillations are observed.

Closer examination of the simulation results discerns, however, some important differences between the two cases. While correlations have an oscillatory behavior in both cases, the corresponding *frequencies* and *amplitudes* are quite different. As discussed in Ref. [18], in the confining case $h > 0$ the frequencies of oscillations scale with $h^{2/3}$ and correspond to bound

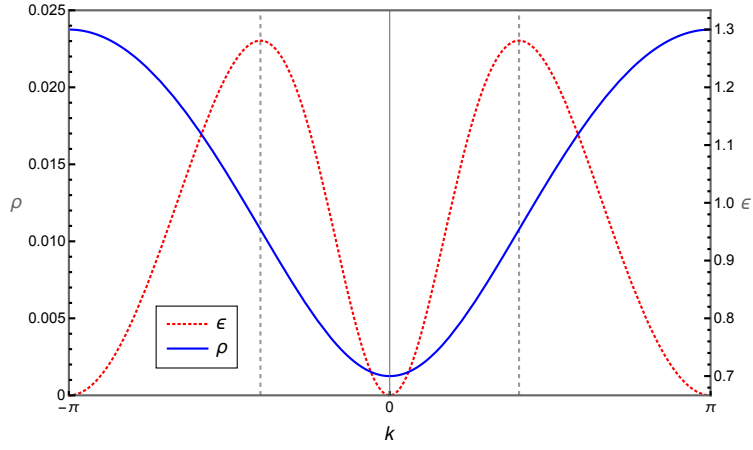


Figure 2.2: The kink dispersion relation $\epsilon(k)$ for $g = 0.3$ and the initial density $\rho(k)$ for $g_0 = 0$, $g = 0.3$.

states of domain walls called “mesons”. In contrast, for the anti-confining case the characteristic frequency scales with h , as shown explicitly by the quench spectroscopy discussed in Subsection 2.4.

2.2 Bloch oscillations

As already stated, oscillations observed for $h < 0$ can be interpreted as Bloch oscillations. They are related to the lattice structure of the model, and can be easily understood within a semi-classical picture. Consider first a pure transverse field quench with $h = 0$ and $g > 0$. The post-quench state then consists of independent kink-antikink pairs with momenta k and $-k$. These kinks behave as non-interacting fermions with a dispersion relation, $\epsilon(k) = 2J\sqrt{1 + g^2 - 2g \cos k}$, and propagate with the group velocity

$$v(k) = \frac{\partial \epsilon(k)}{\partial k} , \quad (2.2)$$

limited by the maximum velocity, $v_{\max} = 2Jg$. The initial density of kinks can be determined following Refs. [15, 34]. Kink-antikink pairs of momentum $\pm k$ are created with a pair creation amplitude, $K(k) = \tan \Delta_k/2$, with

$$\cos \Delta_k = \frac{gg_0 - (g + g_0) \cos k + 1}{\sqrt{1 + g^2 - 2g \cos k} \sqrt{1 + g_0^2 - 2g_0 \cos k}} . \quad (2.3)$$

and the density of kink pairs with momentum in the interval $[k, k + dk]$ is given by

$$\rho(k) = \frac{|K(k)|^2}{1 + |K(k)|^2} = \frac{1 - \cos(\Delta_k)}{2} = \sin^2(\Delta_k/2) , \quad (2.4)$$

shown in Fig. 2.2. The denominator in this equation simply reflects the fermionic nature of kinks, and the spatial bubble density is just the integral of $\rho(k)$,

$$\rho_{\text{bubble}} = \int_0^\pi \frac{dk}{2\pi} \rho(k) . \quad (2.5)$$

Bloch oscillations arise due to the finite longitudinal field, $h < 0$, ignored so far. To a first approximation, we can neglect the correction to the dispersion relation $\epsilon(k)$, and treat the

dynamics of the bubbles as that of a two-particle system, a kink and an antikink interacting via a repulsive potential

$$V(r) = -\chi r, \quad (2.6)$$

where r is the distance between the kinks, and χ the coefficient given by the energy gain of flipping the magnetisation into the external field's direction: $\chi = 2m|h| = 2|h|(1 - g^2)^{1/8}$. The semi-classical equation of motion of the kinks is then written as

$$\dot{r} = 2 \frac{\partial \epsilon(k)}{\partial k}, \quad \dot{k} = -\frac{1}{2} \frac{\partial V}{\partial r} = \frac{\chi}{2}, \quad (2.7)$$

with the factors 2 and 1/2 related to having two mobile kinks. The second equation yields immediately $k(t) = k_0 + \frac{1}{2}\chi t$, and can be used to determine the kink-antikink distance as

$$r(t) = \frac{4}{\chi} [\epsilon(k_0 + \chi t/2) - \epsilon(k_0)] + r_0, \quad (2.8)$$

with r_0 initial size of the bubble (typically of the order of the lattice spacing), and $\pm k_0$ the initial momenta of the kinks. Due to the periodicity of $\epsilon(k)$, the kink velocity reverses sign when the momentum k passes the boundary of the Brillouin zone at $k = \pm\pi$, where the kinks turn back. As a result, kinks return to their original position and collide again after a period $T(k_0)$ when the bubble re-collapses ($r(T(k_0)) \approx 0$). This happens when $k_0 + \chi T(k_0)/2 = 2\pi - k_0$. At this point, the kink and the antikink are reflected, and start off again with the whole cycle repeating as illustrated in Fig. 2.3, causing the bubbles oscillate in time.

In contrast to the idealised single-bubble dynamics shown in Fig. 2.3, the observed oscillations shown on the left of Fig. 2.1 result from a large number of bubbles, each having different initial momenta and initial sizes. Nevertheless, these Bloch oscillations still have a characteristic time. As obvious from Fig. 2.2, (and can be indeed verified by direct calculation, for an initial state with $g_0 = 0$) the kink density is highest around momenta corresponding to v_{\max} , which determines the front line of the bubbles, and thus the overall frequency of oscillations via the condition, $\frac{1}{2}\chi T_B = 2k_0 \approx \pi$ for small g -s, yielding

$$\omega \approx \frac{2\pi}{T_B} = \chi.$$

The presence of a distribution of domain wall momenta leads, however, to a gradual decay of oscillations due to the dependence of the oscillation period and phase on the initial kink momentum. Bubble collisions have a similar, degrading effect on coherent oscillations.

We close this subsection with two interesting observations regarding oscillation decay and collisions:

- Kink-antikink pairs collide once during every oscillation period. They could, in principle, annihilate into mesons then; however our numerics shows no such effect in the accessible time frame, which is consistent with recent findings [35] that the inelastic scattering is very ineffective.

These collisions also give rise to a time delay due to the interaction between kinks. In the case of zero longitudinal field, $h = 0$, however, the kink-antikink scattering amplitude is simply -1 , and there is no time delay. Therefore any time delay introduced by kink collisions is of order h , which we can neglect in the simple semi-classical picture used here.

- Collisions between different bubbles lead to interactions between bubbles, leading to corrections to the simple motion described above. This effect can be neglected if the average spacing between bubbles is larger than their maximum allowed size, which leads to the condition $\rho_{\text{bubble}}^{-1} \gg 2\epsilon(\pi)/\chi$. This requires the longitudinal field to be larger than some minimum value, which can be computed as a function of g and turns out to be much smaller than the fields used in our simulations, where the smallest field was $|h| = 0.05$.

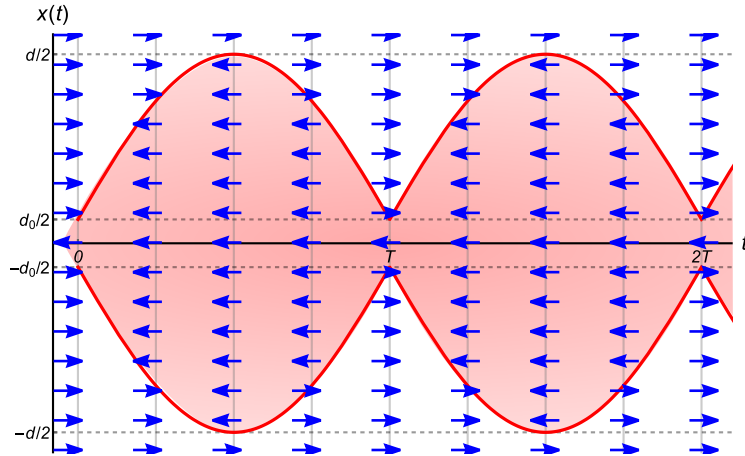


Figure 2.3: Illustrating the Bloch oscillation of a bubble with a definite initial momentum of the kinks forming the bubble walls. Arrows indicate the dominant spin direction as a function of the spatial position for selected time slices. Time delays corresponding to kink collisions are neglected.

2.3 Verifying average bubble size and scaling

One piece of evidence for the suggested scenario is that it predicts an average bubble size that agrees reasonably well with the spatial extension of the correlations. This is demonstrated in Figure 2.1, where the red lines depict the estimate for the average bubble size

$$\langle r \rangle_{\text{anti-conf}} \approx \frac{1}{\rho_{\text{bubble}}} \int_0^\pi \frac{dk_0}{2\pi} \rho(k_0) \frac{4}{\chi} (\epsilon(\pi) - \epsilon(k_0)) \quad (2.9)$$

obtained by neglecting the original bubble size d_0 . For the standard confining case, a similar reasoning gives the average bubble size

$$\langle r \rangle_{\text{conf}} \approx \frac{1}{\rho_{\text{bubble}}} \int_0^\pi \frac{dk_0}{2\pi} \rho(k_0) \frac{4}{\chi} (\epsilon(k_0) - \epsilon(0)) \quad (2.10)$$

since, in this latter case, kink momenta oscillate between k_0 and 0. Note that these estimates depend both on g and h , and give a very good estimate for the spatial extension of the correlations shown in Figure 2.1.

Another tell-tale signal of Bloch oscillations is that their spatial extension is predicted to scale as $\sim 1/h$, while their frequency is proportional to h . This is manifest in the numerically computed time evolution, as demonstrated in Fig. 2.4, where the space-time bubble contour is extracted from the data at $h = -0.1$ and then superimposed on the time evolution obtained for other h values, with time and space rescaled accordingly. Note that the actual distance and time scales vary by a factor of 4, while the correlation profiles remain almost identical when plotted in terms of the scaled variables, $|h|t$ and $|h|l$. This scaling works remarkably well for the first few oscillations. Later differences can be attributed to deviations from our simple semi-classical picture such as the presence of localised spin excitations with frequencies much higher than the Bloch oscillations of the bubble walls, as well as distortions due to bubble collisions and the contributions from the periodic kink collisions when bubbles shrink to their minimal size.

2.4 Quench spectroscopy

‘Quench spectroscopy’, presented in Fig. 2.5, i.e. the Fourier analysis of the time evolution after the quench provides a further tool to assess Bloch oscillations. For small values of $|h|$, we

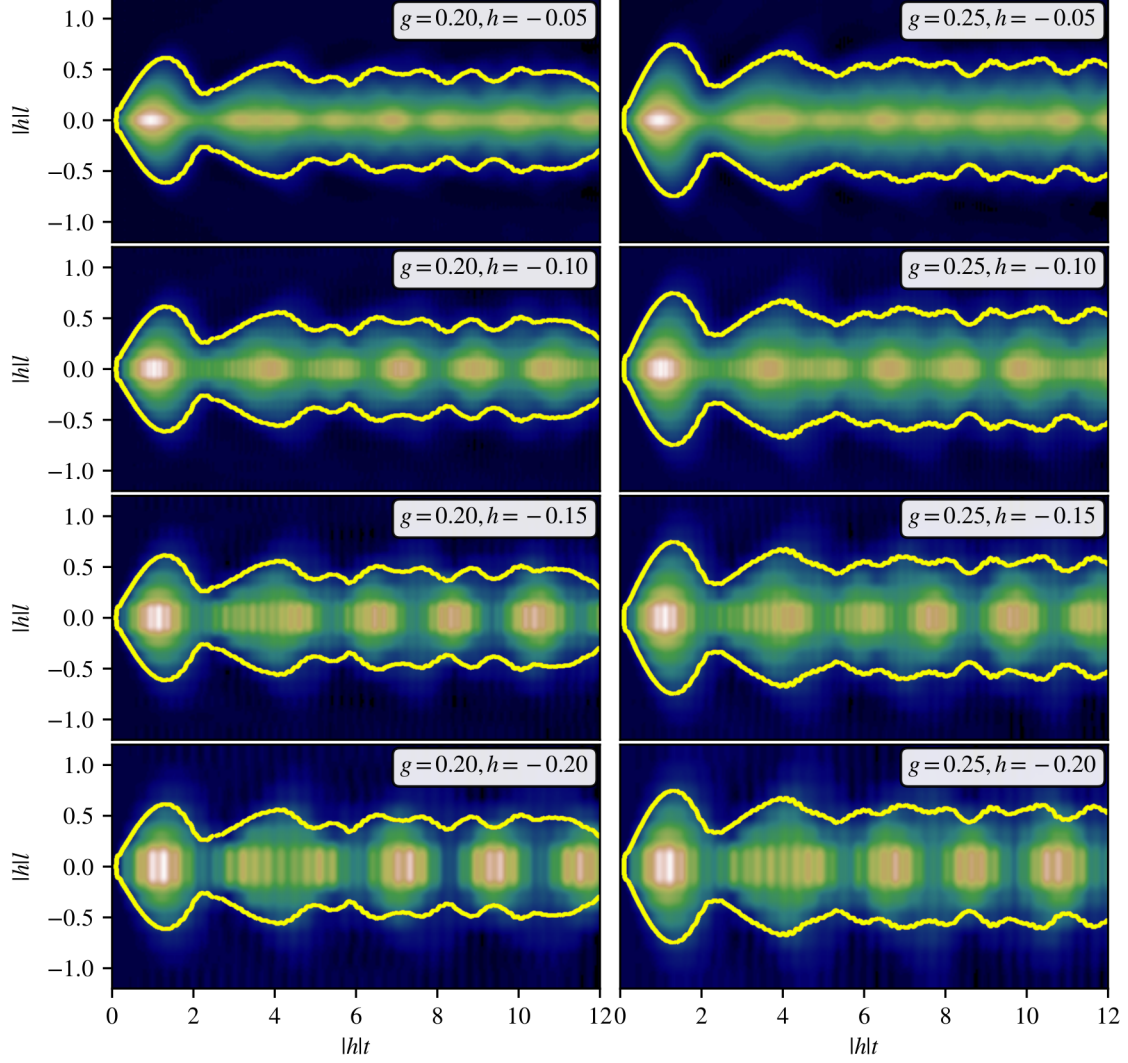


Figure 2.4: Scaling evidence for Bloch oscillations for the transverse field values $g = 0.20$ (left) and $g = 0.25$ (right), with the longitudinal field taking the values $h = -0.05, -0.10, -0.15, -0.20$ for each. The plot shows $\langle \sigma_0^z \sigma_l^z \rangle_c$ as a function of the scaling variables $|h|t$ and $|h|l$. The colour scale is defined by normalising the maximum value of the correlator to 1, while the red lines show the bubble wall defined by the data with $h = -0.10$ at one tenth of its maximum value.

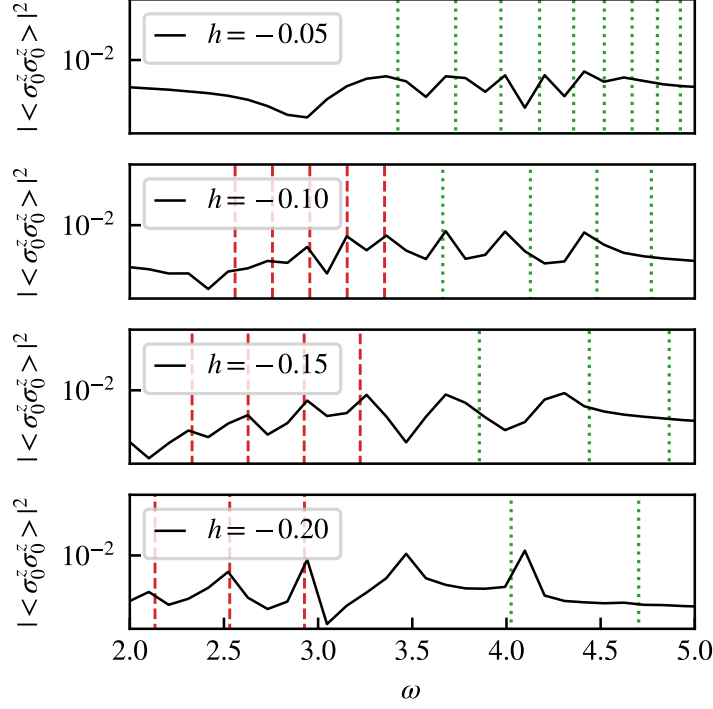


Figure 2.5: Power spectrum of $\langle \sigma_0^z(t) \sigma_l^z(t) \rangle_c$ for $l = 0$ and $g = 0.25$. Green dotted lines show meson frequencies (computed following [18]) - note that they become less and less relevant as $|h|$ grows. Red dashed lines have a spacing $\chi = 2|h|m$, indicating a regular sequence of higher harmonics of the Bloch oscillations, which instead become more prominent for higher values of $|h|$.

only observe frequency peaks corresponding to mesonic bound states. The energy gap of these mesonic excitations is always larger than twice the kink gap, grows with increasing $|h|$, and can also be computed theoretically using a semi-classical method [18, 36]. For small quench fields, we do not observe Bloch oscillations. This is not unexpected, since the bubbles are large, and collide with each other before their oscillation could be observed.

For larger field values, however, mesons are harder to create, and bubble collisions become less frequent. We therefore expect and indeed find that mesonic contributions to the frequency spectrum become less and less pronounced with growing $|h|$, while at the same time another set of regularly spaced frequency peaks emerges well below the threshold of mesonic excitations.

Due to the dependence of their period on the initial kink momentum k_0 , the Bloch oscillations do not in general have a well-defined frequency. Nevertheless, as explained above, we still expect to see a strong feature at the characteristic frequency, $\omega = \chi$. Furthermore, since Bloch oscillations are non-harmonic, the frequency spectrum is expected to contain a regular sequence of higher harmonics. Indeed, such a series of peaks is seen to coincide with the red lines in Fig. 2.5, with the distance between them equal to χ . Note that the simulation can only capture higher harmonics, mostly due to the finite time window of the numerical simulations, but also due to low-frequency background which results from the quench time evolution containing frequencies corresponding to all differences between energy levels of the post-quench Hamiltonian.

3 Conclusions

As we demonstrated in this work within the transverse field Ising model, light-cone time evolution and the decay of the false vacuum can be absent in one-dimensional systems even in a deconfined quench regime, where the formation of bubbles would be energetically favorable. Rather, quite unexpectedly, we observe in this regime spatially confined correlations, oscillating in time. We identify these as Bloch oscillations. These appear due to the underlying lattice and the periodicity of the quasiparticles' dispersion relation in the momentum variable. Our observations are in agreement with recent results obtained in kinetically constrained Rydberg spin systems [37]. However, while in Ref. [37] a special constraint (fine-tuning) was needed to generate Bloch oscillations, here they emerge quite generically, without any constraint in a regime where quasi-particle excitations would naively be expected to speed up and spread correlations over the system.

Our results are relevant for experimental realisations of the tunneling decay of the false vacuum such as put forward in Ref. [38]. We predict that in discrete spin chains, the dynamics after bubble nucleation lead to Bloch oscillations in general, in stark contrast to expectations from continuum quantum field theories. Our results also demonstrate that simple spin chains provide an experimental realisation of Bloch oscillations, which can clearly be identified from the scaling of the space-time dependent spin-spin correlation functions with the applied longitudinal field.

Acknowledgements

This work was partially supported by National Research, Development and Innovation Office (NKFIH) through the OTKA Grant FK 132146, the Hungarian Quantum Technology National Excellence Program, project no. 2017-1.2.1- NKP- 2017-00001, and by the Fund TKP2020 IES (Grant No. BME-IE-NAT), under the auspices of the Ministry for Innovation and Technology. M.A.W. has also been supported by the UNKP-20-4 New National Excellence Program of the Ministry for Innovation and Technology from the source of the National Research, Development and Innovation Fund.

References

- [1] P. Calabrese and J. Cardy, “Time Dependence of Correlation Functions Following a Quantum Quench,” *Phys. Rev. Lett.* **96** (2006) 136801, [arXiv:cond-mat/0601225](#) [[cond-mat.stat-mech](#)].
- [2] P. Calabrese and J. Cardy, “Quantum quenches in extended systems,” *Journal of Statistical Mechanics: Theory and Experiment* **2007** (2007) 06008, [arXiv:0704.1880](#) [[cond-mat.stat-mech](#)].
- [3] T. Kinoshita, T. Wenger, and D. S. Weiss, “A quantum Newton’s cradle,” *Nature* **440** (2006) 900–903.
- [4] S. Hofferberth, I. Lesanovsky, B. Fischer, T. Schumm, and J. Schmiedmayer, “Non-equilibrium coherence dynamics in one-dimensional Bose gases,” *Nature* **449** (2007) 324–327, [arXiv:0706.2259](#) [[cond-mat.other](#)].
- [5] S. Trotzky, Y. A. Chen, A. Flesch, I. P. McCulloch, U. Schollwöck, J. Eisert, and I. Bloch, “Probing the relaxation towards equilibrium in an isolated strongly correlated one-dimensional Bose gas,” *Nature Physics* **8** (2012) 325–330, [arXiv:1101.2659](#) [[cond-mat.quant-gas](#)].

- [6] M. Cheneau, P. Barmettler, D. Poletti, M. Endres, P. Schauß, T. Fukuhara, C. Gross, I. Bloch, C. Kollath, and S. Kuhr, “Light-cone-like spreading of correlations in a quantum many-body system,” *Nature* **481** (2012) 484–487, [arXiv:1111.0776 \[cond-mat.quant-gas\]](#).
- [7] F. Meinert, M. J. Mark, E. Kirilov, K. Lauber, P. Weinmann, A. J. Daley, and H. C. Nägerl, “Quantum Quench in an Atomic One-Dimensional Ising Chain,” *Phys. Rev. Lett.* **111** (2013) 053003, [arXiv:1304.2628 \[cond-mat.quant-gas\]](#).
- [8] T. Langen, R. Geiger, M. Kuhnert, B. Rauer, and J. Schmiedmayer, “Local emergence of thermal correlations in an isolated quantum many-body system,” *Nature Physics* **9** (2013) 640–643, [arXiv:1305.3708 \[cond-mat.quant-gas\]](#).
- [9] T. Langen, S. Erne, R. Geiger, B. Rauer, T. Schweigler, M. Kuhnert, W. Rohringer, I. E. Mazets, T. Gasenzer, and J. Schmiedmayer, “Experimental observation of a generalized Gibbs ensemble,” *Science* **348** (2015) 207–211, [arXiv:1411.7185 \[cond-mat.quant-gas\]](#).
- [10] A. M. Kaufman, M. E. Tai, A. Lukin, M. Rispoli, R. Schittko, P. M. Preiss, and M. Greiner, “Quantum thermalization through entanglement in an isolated many-body system,” *Science* **353** (2016) 794–800, [arXiv:1603.04409 \[quant-ph\]](#).
- [11] E. H. Lieb and D. W. Robinson, “The finite group velocity of quantum spin systems,” *Communications in Mathematical Physics* **28** (1972) 251–257.
- [12] F. Iglói and H. Rieger, “Long-Range Correlations in the Nonequilibrium Quantum Relaxation of a Spin Chain,” *Phys. Rev. Lett.* **85** (2000) 3233–3236.
- [13] A. M. Läuchli and C. Kollath, “Spreading of correlations and entanglement after a quench in the one-dimensional Bose Hubbard model,” *Journal of Statistical Mechanics: Theory and Experiment* **2008** (2008) 05018.
- [14] S. R. Manmana, S. Wessel, R. M. Noack, and A. Muramatsu, “Time evolution of correlations in strongly interacting fermions after a quantum quench,” *Phys. Rev. B* **79** (2009) 155104, [arXiv:0812.0561 \[cond-mat.str-el\]](#).
- [15] P. Calabrese, F. H. L. Essler, and M. Fagotti, “Quantum Quench in the Transverse-Field Ising Chain,” *Phys. Rev. Lett.* **106** (2011) 227203, [arXiv:1104.0154 \[cond-mat.str-el\]](#).
- [16] L. Bonnes, F. H. L. Essler, and A. M. Läuchli, ““Light-Cone” Dynamics After Quantum Quenches in Spin Chains,” *Phys. Rev. Lett.* **113** (2014) 187203, [arXiv:1404.4062 \[cond-mat.str-el\]](#).
- [17] G. Carleo, F. Becca, L. Sanchez-Palencia, S. Sorella, and M. Fabrizio, “Light-cone effect and supersonic correlations in one- and two-dimensional bosonic superfluids,” *Phys. Rev. A* **89** (2014) 031602.
- [18] M. Kormos, M. Collura, G. Takács, and P. Calabrese, “Real-time confinement following a quantum quench to a non-integrable model,” *Nature Physics* **13** (2017) 246–249, [arXiv:1604.03571 \[cond-mat.stat-mech\]](#).
- [19] G. Magnifico, M. Dalmonte, P. Facchi, S. Pascazio, F. V. Pepe, and E. Ercolessi, “Real Time Dynamics and Confinement in the \mathbb{Z}_n Schwinger-Weyl lattice model for 1+1 QED,” *arXiv e-prints* (2019) arXiv:1909.04821, [arXiv:1909.04821 \[quant-ph\]](#).

- [20] W. L. Tan, P. Becker, F. Liu, G. Pagano, K. S. Collins, A. De, L. Feng, H. B. Kaplan, A. Kyprianidis, R. Lundgren, W. Morong, S. Whitsitt, A. V. Gorshkov, and C. Monroe, “Observation of Domain Wall Confinement and Dynamics in a Quantum Simulator,” *arXiv e-prints* (2019) arXiv:1912.11117, [arXiv:1912.11117 \[quant-ph\]](#).
- [21] P. P. Mazza, G. Peretto, A. Leroose, M. Collura, and A. Gambassi, “Suppression of transport in nondisordered quantum spin chains due to confined excitations,” *Phys. Rev. B* **99** (2019) 180302, [arXiv:1806.09674 \[cond-mat.stat-mech\]](#).
- [22] N. J. Robinson, A. J. A. James, and R. M. Konik, “Signatures of rare states and thermalization in a theory with confinement,” *Phys. Rev. B* **99** (2019) 195108, [arXiv:1808.10782 \[cond-mat.str-el\]](#).
- [23] A. J. A. James, R. M. Konik, and N. J. Robinson, “Nonthermal States Arising from Confinement in One and Two Dimensions,” *Phys. Rev. Lett.* **122** (2019) 130603, [arXiv:1804.09990 \[cond-mat.stat-mech\]](#).
- [24] F. Liu, R. Lundgren, P. Titum, G. Pagano, J. Zhang, C. Monroe, and A. V. Gorshkov, “Confined Quasiparticle Dynamics in Long-Range Interacting Quantum Spin Chains,” *Phys. Rev. Lett.* **122** (2019) 150601, [arXiv:1810.02365 \[cond-mat.quant-gas\]](#).
- [25] J. Vovrosh and J. Knolle, “Confinement and Entanglement Dynamics on a Digital Quantum Computer,” *arXiv e-prints* (2020) arXiv:2001.03044, [arXiv:2001.03044 \[cond-mat.str-el\]](#).
- [26] A. Leroose, F. M. Surace, P. P. Mazza, G. Peretto, M. Collura, and A. Gambassi, “Quasilocalized dynamics from confinement of quantum excitations,” *Phys. Rev. B* **102** (2020) 041118, [arXiv:1911.07877 \[cond-mat.stat-mech\]](#).
- [27] T. Chanda, J. Zakrzewski, M. Lewenstein, and L. Tagliacozzo, “Confinement and Lack of Thermalization after Quenches in the Bosonic Schwinger Model,” *Phys. Rev. Lett.* **124** (2020) 180602, [arXiv:1909.12657 \[cond-mat.stat-mech\]](#).
- [28] Z.-C. Yang, F. Liu, A. V. Gorshkov, and T. Iadecola, “Hilbert-Space Fragmentation from Strict Confinement,” *Phys. Rev. Lett.* **124** (2020) 207602, [arXiv:1912.04300 \[cond-mat.str-el\]](#).
- [29] B. M. McCoy and T. T. Wu, “Two-dimensional Ising field theory in a magnetic field: Breakup of the cut in the two-point function,” *Phys. Rev. D* **18** (1978) 1259–1267.
- [30] S. Coleman, “Fate of the false vacuum: Semiclassical theory,” *Phys. Rev. D* **15** (1977) 2929–2936.
- [31] J. Callan, Curtis G. and S. Coleman, “Fate of the false vacuum. II. First quantum corrections,” *Phys. Rev. D* **16** (1977) 1762–1768.
- [32] R. J. V. Tortora, P. Calabrese, and M. Collura, “Relaxation of the order-parameter statistics and dynamical confinement,” *arXiv e-prints* (2020) arXiv:2005.01679, [arXiv:2005.01679 \[cond-mat.stat-mech\]](#).
- [33] G. Vidal, “Efficient Simulation of One-Dimensional Quantum Many-Body Systems,” *Phys. Rev. Lett.* **93** (2004) 040502, [arXiv:quant-ph/0310089 \[quant-ph\]](#).

- [34] P. Calabrese, F. H. L. Essler, and M. Fagotti, “Quantum quench in the transverse field Ising chain: I. Time evolution of order parameter correlators,” *Journal of Statistical Mechanics: Theory and Experiment* **2012** (2012) 07016, [arXiv:1204.3911 \[cond-mat.quant-gas\]](#).
- [35] A. Milsted, J. Liu, J. Preskill, and G. Vidal, “Collisions of false-vacuum bubble walls in a quantum spin chain,” *arXiv e-prints* (2020) arXiv:2012.07243, [arXiv:2012.07243 \[quant-ph\]](#).
- [36] S. B. Rutkevich, “Large-n Excitations in the Ferromagnetic Ising Field Theory in a Weak Magnetic Field: Mass Spectrum and Decay Widths,” *Phys. Rev. Lett.* **95** (2005) 250601, [arXiv:hep-th/0509149 \[hep-th\]](#).
- [37] M. Magoni, P. P. Mazza, and I. Lesanovsky, “Emergent Bloch oscillations in a kinetically constrained Rydberg spin lattice,” *Phys. Rev. Lett.* **126** (2021) 103002, [arXiv:2010.07825 \[cond-mat.quant-gas\]](#).
- [38] S. Abel and M. Spannowsky, “Quantum-field-theoretic simulation platform for observing the fate of the false vacuum,” *PRX Quantum* **2** (2021) 010349, [arXiv:2006.06003 \[hep-th\]](#).